On the Crucial Impact of Antennas and Diversity on BLE RSSI-based Indoor Localization

Henry Schulten[1], Marc Kuhn[1], Robert Heyn[1], Gregor Dumphart[1], Florian Trösch[2], and Armin Wittneben[1]

[1]Communication Technology Laboratory, ETH Zurich, Switzerland

[2]The PORT Technology, Schindler Aufzüge AG, Switzerland

E-Mail: {schulten, kuhn, heyn, dumphart, wittneben}@nari.ee.ethz.ch, florian.troesch@schindler.com

Abstract—Due to their low complexity, RSSI-based solutions for indoor localization have become increasingly popular in recent years despite lacking the accuracy of more sophisticated localization solutions. One of the main reasons for this lack of accuracy is the highly fluctuating nature of RSSI values as a result of indoor channel characteristics, hardware imperfections and varying antenna radiation patterns. In this paper, we thus critically analyze the log-normal path loss model and its validity with the focus on indoor localization. We show how chip antennas of typical consumer devices affect the RSSI measurements and clarify in what manner this effect can be incorporated into the log-normal model. In this process, we are also able to quantify the impact of small-scale fading and diversity on RSSI-based distance estimation. We furthermore propose a novel calibration scheme that estimates path loss exponents based on a simple training walk and outperforms linear regression in all our use cases. At last, we combine our findings in an implementation of an indoor localization system for a 14×3 m office corridor. On average, our measurements yield a significantly decreased position RMSE of 1.36 m, which compares to the Cramér-Rao lower bound on the position RMSE of 0.71 m in this environment.

Index Terms—Antenna, Bluetooth, Distance Estimation, Localization, Path Loss, RSSI, Tracking

I. INTRODUCTION

Bluetooth Low Energy (BLE) has been studied intensively for localization and user tracking in recent years. Its low complexity due to the readily available Received Signal Strength Indicator (RSSI) measurements, the low power consumption, ubiquitous availability, low cost and the ease of device deployment make it an attractive technology for localization. However, indoor channel characteristics such as frequency-selective small-scale fading, that affects the three advertising channels of BLE distinctively, and shadowing cause strong fluctuations of the RSSI observations. Moreover, the direction-dependent antenna radiation patterns that are typical for handheld devices further affect the RSSI values in a variable manner and introduce even more ambiguities. Since the resulting unreliable RSSI observations are used for the distance estimation between transmitting agents (operating as BLE advertiser) and receiving anchors (operating as BLE observers), the achievable ranging and localization accuracy is severely limited. In this paper we thus investigate whether the popular log-normal path loss model (PLM) is a sufficient statistical representation when

using common BLE devices and to what extend diversity and calibration can mitigate the arising inaccuracies. Our goal is then to enhance the localization accuracy of BLE RSSI-based indoor systems and to obtain insights on the remaining limiting factors.

Selected related work: The background and characteristics of different types of indoor and outdoor PLMs are discussed thoroughly in various standard textbooks, e.g. in [1], which also states that an advantage of simple statistical models is their broader applicability and compactness. Dong and Dargie [2] evaluated the usability of 802.15.4 radio RSSI values for indoor distance estimation based on the popular log-normal PLM and deemed this approach futile. However, they did not consider the possible influence of varying antenna radiation patterns of their devices and also focused on very large agent-anchor distances of up to 30 m. The impact of antenna polarization and orientation on RSSI values was analyzed in [3] and shown to be significant, but the used antennas were similar to dipoles and the orientation of the devices was assumed to be known. This enabled a specific deterministic model that might not be applicable in general. RSSI-based localization by multilateration of log-normal PLM based distance estimates was studied in [4], [5], where it was attempted to combat the RSSI inaccuracies by Kalman filter smoothing of past values [5] or by sensor fusion of additional side information [4]. The results of these studies were more accurate than the prior unprocessed estimation approaches but had higher complexity demands.

Contribution of this work: We put the log-normal PLM in perspective and state it in a more general form, where the influences of small-scale fading, shadowing, and antenna radiation patterns are clearly separated. In this context, we observe that the orientation of on-chip antennas can lead to RSSI drops of up to 37 dB. However, by statistical analysis of the radiation patterns, we show that it is possible to incorporate their effect into the existing log-normal PLM by including another log-normal random variable. We furthermore analyze the impact of diversity on the accuracy of distance estimates and find that moderate diversity orders of 3 to 4 already significantly reduce the root mean squared error (RMSE). We also introduce a novel calibration scheme to estimate path loss exponents of the PLM based on a simple training walk. This calibration further increases the accuracy of the distance estimation by adjusting it to different propagation scenarios.

Furthermore, we apply the corresponding maximum likelihood (ML) estimator of the PLM for actual user localization in an office corridor. These measurement-based results are discussed and compared to both conventional multilateration as well as the Cramér-Rao lower bound on the position RMSE for unbiased position estimators.

II. Path Loss Model

In radio communications, it is common practice to relate the received signal power $P_R(d)$ for variable distances d to the received power $P_{R,d_0} = P_R(d_0)$ at a fixed distance d_0 via [6]

$$P_R(d) = P_{R,d_0} \frac{xsg}{\left(\frac{d}{d_0}\right)^\alpha}. \tag{1}$$

Thereby, $\alpha > 0$ is the environment-dependent path loss exponent. Furthermore, x represents small-scale fading due to multipath propagation and s models possible shadowing due to objects blocking the line-of-sight (LOS) path. The variable g accounts for the product of transmit and receive antenna gain. In the light of non-isotropic antenna radiation patterns, which are typical for off-the-shelf chip antennas, g depends on the orientation of both transmitter and receiver. Since these orientations are unknown and change with movement of either device, we model g as a random variable rather than a constant. Transforming (1) to the decibel (dB) scale leads to

$$\text{RSSI}(d) = \text{RSSI}_{d_0} - 10\alpha \log_{10}\left(\frac{d}{d_0}\right) + W \tag{2}$$

with $\text{RSSI}_{d_0} = 10 \log_{10}(P_{R,d_0})$ and

$$W = X + S + G \tag{3}$$
$$= 10 \log_{10}(x) + 10 \log_{10}(s) + 10 \log_{10}(g). \tag{4}$$

For the specific case of $W \sim \mathcal{N}(0, \sigma_W^2)$, Equation (2) is referred to as log-normal shadowing PLM.

It was often shown (e.g. by [7]) that S can be modelled as normally distributed. However, X is usually assumed to be logarithmic scaled-χ^2-distributed based on $x = \frac{1}{L} \sum_{i=1}^{L} |h_i|^2$, where $h_i \sim \mathcal{CN}(\mu_h, \sigma_h^2)$ (Rayleigh or Rician fading), which would lead to an overall non-normal distribution. Even so, it is intuitive that exploiting a high number of diversity branches L recovers the normal properties of $X + S$ as $X \to \text{const.}$ Nevertheless, even with sufficient diversity, the PDF of G still needs to be investigated in order to draw conclusions about the overall statistics of W.

To this end, we conducted measurements with a BLE advertising iPhone 6 [8] as agent and identical Raspberry Pis [9] as receiving anchors[1]. The devices were set up in an anechoic chamber to eliminate the effect of small-scale fading X, and the shadowing S was mitigated by ensuring an unobstructed line-of-sight (LOS) path. The 2D radiation patterns of the transmitter and the receiver were recorded at distance $d = 1$ m and are shown in Fig. 1. The resulting normalized histogram of all possible orientation combination

[1]Measurements with an iPod [10] and other BLE chips yield similar results.

of these two patterns is depicted in Fig. 2. The histogram resembles a normal distribution and, assuming that each of these combinations is equally likely, properly illustrates the empirical PDF of G (without mean). The standard deviation of the normal perturbation G that is caused by the random antenna orientations on both transmitter and receiver side amounts to $\sigma_G = 6.49$ dB. It can be reduced significantly if we limit the random antenna orientation to an angular range of less than $360°$ (sectorization). To this end, Fig. 3 shows the resulting σ_G as a function of the sector width on both sides. Typical values for our setups are $50°$ - $100°$ for the Raspberry Pis and $50°$ - $200°$ for the mobile agent (red box), which corresponds to $\sigma_G \approx 4$ dB. By inspection of the corresponding histograms (not shown), we conclude that for randomly selected sector widths larger than $50°$ for the considered antennas, the log-normal PLM appears appropriate, even in LOS scenarios.
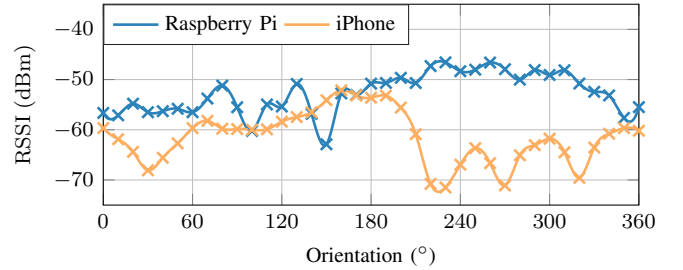

Fig. 1: Interpolated antenna radiation patterns (RSSI) of Raspberry Pi and iPhone 6.
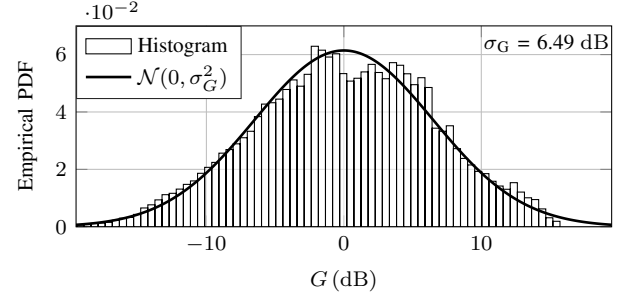

Fig. 2: Zero-mean histogram of the resulting attenuation of every possible antenna orientation combination and normal approximation for the empirical PDF of G.
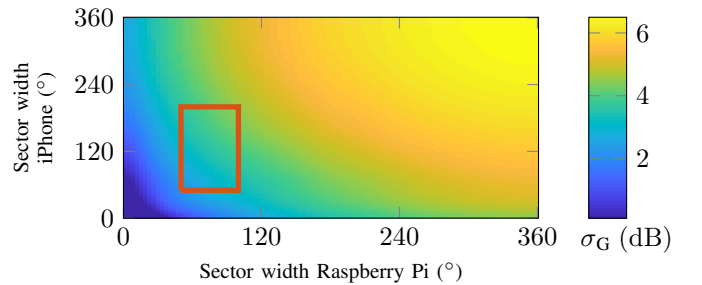

Fig. 3: Impact of sector width on σ_G and typical area of operation (red box).

After motivating that G can be assumed to be normally distributed, we can consequently adjust (2) to

$$\text{RSSI}(d) = \overline{\text{RSSI}}_{d_0} - 10\alpha \log_{10}\left(\frac{d}{d_0}\right) + \tilde{W} \qquad (5)$$

with $\overline{\text{RSSI}}_{d_0} = \text{RSSI}_{d_0} + \mu_G$ now including the mean of the radiation patterns $\mu_G = \mu_W$ (cf. Tab. I), such that $\tilde{W} \sim \mathcal{N}(0, \sigma_{\tilde{W}}^2 = \sigma_X^2 + \sigma_S^2 + \sigma_G^2)$. The log-normal PLM thus remains a valid representation of the occurring indoor effects when considering typical BLE chip antennas.

TABLE I: Overview of random variables.

Effect	Variable	PDF
Shadowing	S	$f_S(S) = \mathcal{N}(S; 0, \sigma_S^2)$
Radiation patterns	G	$f_G(G) = \mathcal{N}(G; \mu_G, \sigma_G^2)$
Small-scale fading	X	$f_X(X; L) \overset{L \gg 1}{\approx} \mathcal{N}(X; 0, \sigma_X^2)$
Overall	W	$f_W(W) = \mathcal{N}(W; \mu_W, \sigma_W^2)$
Overall (zero mean)	$\tilde{W}$	$f_{\tilde{W}}(\tilde{W}) = \mathcal{N}(\tilde{W}; 0, \sigma_{\tilde{W}}^2)$

III. IMPACT OF DIVERSITY ON DISTANCE ESTIMATION

While it was mentioned that model (5) is only valid with sufficient diversity, the exact impact of increasing diversity order L and how to achieve it is yet left unclear. Fig. 4 motivates the importance of diversity, showing measured RSSI values over distance for a constant device orientation, clear LOS, and $L = 1$ or $L = 4$ for an indoor channel with strong multipath characteristic. It can be seen that deep fades (significant drops of the RSSI, e.g. at $d = 1$ m) are present for diversity order $L = 1$. These deep fades lead to drastic overestimation of the distance and render the associated estimates useless.
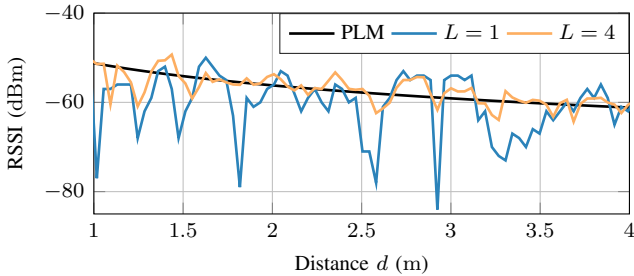

Fig. 4: Exemplary measurements with diversity orders $L = 1$ (blue) and $L = 4$ (yellow) compared to the mean of the log-normal PLM (black).

In order to properly quantify the mismatch that is caused by the residual small-scale fading x, we apply the log-normal ML distance estimator of (5) in the presence of small diversity factors L, i.e., we let $\frac{2L}{\sigma_h^2}x \sim \chi^2(2L, \lambda)$ and define $S + G - \mu_G =: N \sim \mathcal{N}(0, \sigma_N^2 = \sigma_S^2 + \sigma_G^2)$. Note that diversity can be obtained in the spatial (antennas), spectral (frequency slots) and temporal (time) domain by averaging the corresponding linear RSSI measurements. We assume that all RSSI measurements in the same averaging window are subject to the same shadowing, antenna gains, and path loss.

Thus, diversity does not affect the PDF of N. The ML estimate follows as [11]

$$\hat{d}_{\text{ML}} = d_0 10^{\frac{\overline{\text{RSSI}}_{d_0} - \text{RSSI}(d)}{10\alpha}} \qquad (6)$$

$$= d\, x^{-\frac{1}{\alpha}} 10^{-\frac{N}{10\alpha}}. \qquad (7)$$

With statistical independence between N and x, we can hence write the relative distance MSE $\varepsilon_{\text{nMSE}}$ as

$$\varepsilon_{\text{nMSE}} = \frac{1}{d^2}\, \text{E}\left[\left(\hat{d}_{\text{ML}} - d\right)^2\right] \qquad (8)$$

$$= 1 + \text{E}\left[x^{-\frac{2}{\alpha}}\right]\text{E}\left[10^{-\frac{2N}{10\alpha}}\right] - 2\,\text{E}\left[x^{-\frac{1}{\alpha}}\right]\text{E}\left[10^{-\frac{N}{10\alpha}}\right] \qquad (9)$$

$$= 1 + \varepsilon_x\left(L, \frac{\alpha}{2}\right)\varepsilon_N\left(\frac{\alpha}{2}\right) - 2\,\varepsilon_x(L, \alpha)\,\varepsilon_N(\alpha). \qquad (10)$$

For $L > \frac{2}{\alpha}$ and Rayleigh fading (i.e. $\mu_h = 0$, $\lambda = 0$) its components are given by (cf. Appendix A and [11])

$$\varepsilon_x(L, \alpha) = \left(\frac{L}{\sigma_h^2}\right)^{\frac{1}{\alpha}}\frac{\Gamma\left(L - \frac{1}{\alpha}\right)}{\Gamma(L)} \qquad (11)$$

$$\varepsilon_N(\alpha) = \exp\left(\frac{\ln(10)^2}{100}\frac{\sigma_N^2}{2\alpha^2}\right). \qquad (12)$$

Fig. 5 shows the resulting relative RMSE. The black line represents the combined RMSE $\sqrt{\varepsilon_{\text{nMSE}}}$ with both antenna impacts as well as small-scale fading present. The blue and yellow line on the other hand show how the individual perturbations affect the RMSE. Lastly, the dashed green line shows at which diversity order the inclusion of small-scale fading doubles the RMSE. We can also see the drastic loss of accuracy that small-scale fading causes if no diversity is utilized. Due to the previously mentioned assumptions, the antenna impact does not depend on the diversity order. The combined RMSE for high diversity orders thus approaches the error that we obtain due to the non-isotropic antenna patterns. We conclude that in our use cases with $\sigma_N \approx \sigma_G \approx 4\,\text{dB}$ (cf. Fig. 3), 3 or 4 diversity branches are sufficient to neglect small-scale fading. Furthermore, it becomes clear that the anchors with higher distance to the agent are less reliable, as the RMSE grows linearly (cf. (8)-(10)) with increasing distance.
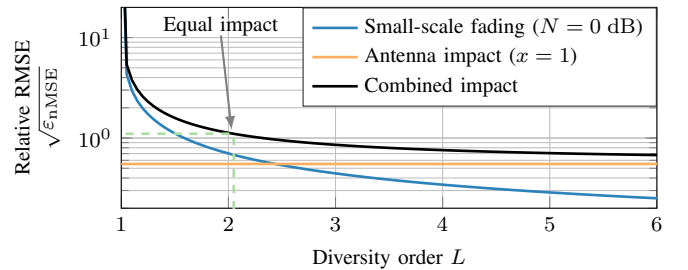

Fig. 5: Relative RMSE of ML distance estimate based on (8) - (12) with $\sigma_h = 1$, $\sigma_N = 4\,\text{dB}$ and $\alpha = 2$.

IV. Position Estimation

As first option (P_1) for the position estimation we will use the typical multilateration (abbr. $\hat{\mathbf{p}}_{\mathrm{LS}}$) of the individual ML distance estimates. This estimator coincides with the ML position estimator for situations in which the distance estimates are subject to i.i.d. AWGN and is given by

$$\hat{\mathbf{p}}_{\mathrm{LS}} = \underset{\mathbf{p}}{\arg\min} \left\{ \sum_{i=1}^{N_A} \left[\hat{d}_{\mathrm{ML},i} - d_i(\mathbf{p}) \right]^2 \right\} \qquad (13)$$

with $d_i(\mathbf{p})$ being the Euclidean distance from the trial agent position $\mathbf{p}$ to the i-th anchor and N_A as the total number of anchors.

As second option (P_2), we want to use the ML position estimator that is based on the log-normal PLM. In order to obtain this estimator, we first extend the PLM (5) to the vectorial notation $\mathbf{r} = \bar{\mathbf{r}}(\mathbf{p}) + \tilde{\mathbf{w}}$ by denoting

$$\mathbf{r} = [\mathrm{RSSI}_1, ..., \mathrm{RSSI}_{N_A}]^{\mathrm{T}} \quad \text{in dB} \qquad (14)$$

$$\tilde{\mathbf{w}} = \left[\tilde{W}_1, ..., \tilde{W}_{N_A} \right]^{\mathrm{T}} \sim \mathcal{N}(\mathbf{0}, \boldsymbol{\Sigma}_{\tilde{\mathbf{W}}}) \qquad (15)$$

$$\bar{r}_i(\mathbf{p}) = \overline{\mathrm{RSSI}}_{d_0,i} - 10\alpha_i \log_{10}\left(\frac{d_i(\mathbf{p})}{d_0} \right) \qquad (16)$$

$$\bar{\mathbf{r}}(\mathbf{p}) = [\bar{r}_1(\mathbf{p}), ..., \bar{r}_{N_A}(\mathbf{p})]^{\mathrm{T}} . \qquad (17)$$

Here, $\boldsymbol{\Sigma}_{\tilde{W}}$ is the covariance matrix for the respective RVs of the separate anchors. The PLM-based ML position estimator $\hat{\mathbf{p}}_{\mathrm{ML}}$ can consequently be obtained by minimizing the negative log-likelihood function of the according conditional PDF $f_{\mathbf{r}|\mathbf{p}}(\mathbf{r} \mid \mathbf{p})$:

$$\hat{\mathbf{p}}_{\mathrm{ML}} = \underset{\mathbf{p}}{\arg\min} \left\{ [\mathbf{r} - \bar{\mathbf{r}}(\mathbf{p})]^{\mathrm{T}} \boldsymbol{\Sigma}_{\tilde{\mathbf{W}}}^{-1} [\mathbf{r} - \bar{\mathbf{r}}(\mathbf{p})] \right\} \qquad (18)$$

$$\overset{*}{=} \underset{\mathbf{p}}{\arg\min} \left\{ \sum_{i=1}^{N_A} \frac{1}{\sigma_{\tilde{W}_i}^2} [\mathrm{RSSI}_i - \bar{r}_i(\mathbf{p})]^2 \right\} \qquad (19)$$

$$= \underset{\mathbf{p}}{\arg\min} \left\{ \sum_{i=1}^{N_A} \frac{\alpha_i^2}{\sigma_{\tilde{W}_i}^2} \left[\log \hat{d}_{\mathrm{ML},i} - \log d_i(\mathbf{p}) \right]^2 \right\} . \qquad (20)$$

Note that ($*$) holds if the log-normal noise and thus the elements of $\tilde{\mathbf{w}}$ are independent for each anchor.

V. Calibration

In order to apply the position estimators of Section IV, we need to estimate the PLM parameters $\mathrm{RSSI}_{d_0,i}$ and α_i for each anchor i. This is the task of the calibration procedure. This procedure is based on a 'calibration walk', which consists of multiple RSSI measurements at all anchors for a mobile agent with known trajectory. In our reference implementation, denoted *REF*, we used linear ordinary least-squares (OLS) regression to fit the model parameters (RSSI in dB). However, while $\mathrm{RSSI}_{d_0,i}$ is mostly a device dependent parameter, α_i depends on the specific environment and may thus also vary over longer distances or time. Moreover, an adaptive choice for the path loss exponents could also capture the effect of static obstacles or mitigate the impact of the varying antenna patterns (cf. Fig. 3).

Based on these considerations, we propose an improved calibration scheme in the sequel. This new scheme is referred to as *mean RSSI method* (*MRM*) and does not rely on OLS regression over an entire training walk. Instead, we calculate distinct path loss exponents $\alpha_{i,k}$ for each anchor $i = 1, ..., N_A$ and for $k = 1, ..., N_C$ individually chosen segments (*chunks*) of the training walk (see Fig. 6). We assume that these segments are chosen small enough for the path loss exponents to remain constant. We furthermore expect $\overline{\mathrm{RSSI}}_{d_0,i}$ to be constant, known and equal for all anchors. Based on the Gaussian assumption from (5), the according ML estimate of the path loss exponents for the fixed offset $\overline{\mathrm{RSSI}}_{d_0}$ is then given by

$$\hat{\alpha}_{i,k} = \frac{\sum_{j=1}^{N_S} \log_{10}\left(\frac{d_{i,k,j}}{d_0} \right) \left(\overline{\mathrm{RSSI}}_{d_0} - \mathrm{RSSI}_{i,k,j} \right)}{10 \cdot \sum_{j=1}^{N_S} \log_{10}^2 \left(\frac{d_{i,k,j}}{d_0} \right)} \qquad (21)$$

where $j = 1, ..., N_S$ refers to the j-th measurement in the respective chunk and for the respective anchor. Thereby $d_{i,k,j}$ follows from the known agent position for each tupel (i, k, j).

The mean RSSI values $\overline{\mathrm{RSSI}}_{i,k} = \frac{1}{N_S} \sum_{j=1}^{N_S} \mathrm{RSSI}_{i,k,j}$ of each anchor and chunk are furthermore saved and used as situation indicators[2] that allow us to choose which of the recorded parameter sets to use for each distance estimation.
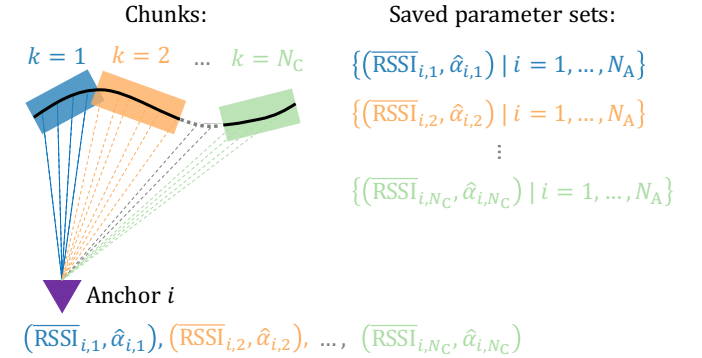

Fig. 6: Schematic illustration of a *MRM* calibration walk with arbitrary but known true path (black) that is separated into N_C chunks. For simplicity only anchor i is shown.

In order to get some insight into the performance of the *MRM* and *REF* calibration we performed a calibration walk in the corridor shown in Fig. 8. In this test walk, the mobile agent moved from the back to the front along the center line and with a constant velocity. The black curve in the lower plot of Fig. 7 shows the evolution of the agent's distance to the center lefthand anchor (red box) over time. The blue curve shows the distance estimates obtained with the parameter sets from the *REF* calibration, while the yellow curve relates to the *MRM* with $N_C = 6$ chunks. The distance RMSE in this example is reduced remarkably from $5.2\,\mathrm{m}$ to $1.4\,\mathrm{m}$.

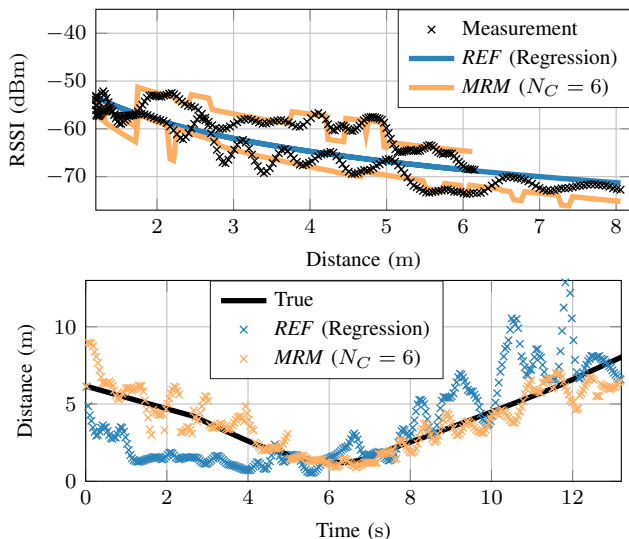[2]We use the mean RSSI values for joint RSSI fingerprinting to roughly select in which chunk the user might be.

Fig. 7: RSSI comparison (top) and distance estimation (bottom) for a straight corridor walk. *REF* calibration (blue with RMSE of $5.2\,\mathrm{m}$) vs. *MRM* calibration (yellow with RMSE of $1.4\,\mathrm{m}$).

Fig. 8: Anchor constellation for the corridor setup.

Moreover, the black curve in the upper plot of Fig. 7 shows the measured RSSI values[3] as a function of the distance to the center lefthand anchor. The upper black curve relates to the part of the trajectory towards the anchor, whereas the lower black curve relates to the part away from the anchor. Based on the REF parameter set, the RSSI values predicted by the model (blue) do not reflect these two different cases. In contrast, the *MRM* based parameter set with chunks (yellow) is clearly able to separate between the two different scenarios and predicts the measured RSSI values far more accurately. Note that the two different propagation scenarios are probably due to the LOS while moving towards the anchor and the user's body shadowing the LOS while moving away.

VI. LOCALIZATION RESULTS

Ultimately, we compare the localization performance of both calibration schemes (*REF* and *MRM*) for the position estimators P_1 and P_2 from Section IV in the corridor setup from Fig. 8. Based on the previous findings, we exploited $L = 4$ diversity branches by spatial and time diversity in order to mitigate small-scale fading. The exemplary results[4] for the tracking of a zigzag trajectory with chosen average anchor density of $\rho \approx 0.14\,\mathrm{m}^{-2}$ are shown in Fig. 9 and Fig. 10, where they are also compared to the corresponding averaged position error bound (PEB, cf. [12]). The required covariance matrix $\Sigma_{\bar{W}}$ for the PEB (cf. (15)) was evaluated based on previous measurements with known trajectories. The black line of the plot represents the true walk, whose trajectory

was directed from one anchor to the next with abrupt changes in orientation. We can see that many estimates obtained by the *REF* / P_1 scheme lie outside of the corridor and that no clear path can be reconstructed by using them, rendering them almost useless for indoor localization. The proposed localization *MRM* / P_2 on the other hand matches the correct path and could be used to decide whether an object moves into a certain direction. However, the RMSE for this walk is still $39\,\mathrm{cm}$ larger than the according averaged PEB.

Moreover, analyzing the ellipses of the PEB for some positions confirms three expectations. First, the position error along the radial axis of the closest anchors is generally smaller than in orthogonal direction, leading to a higher possible accuracy along this axis. Second, this accuracy increases drastically the closer one gets to the closest anchor, while the effect of the other anchors is subordinate, meaning that closer anchors have a higher reliability. Lastly, the PEB is significantly smaller if one is surrounded by anchors, which indicates that higher anchor densities further increase the accuracy and stability of the system.

In order to generalize the numerical results, Tab. II shows the overall results for tracking nine completely different trajectories (including diagonal through the corridor, reverse directions, entering an office) through the same corridor while still relying on the previous calibration walk. The suggested calibration and position estimation *MRM* / P_2 reduces the position RMSE by an impressive 61% to a value of $1.36\,\mathrm{m}$.

TABLE II: General RMSE comparison.

Method	Position RMSE
REF / P_1	$3.51\,\mathrm{m}$
MRM / P_2	$1.36\,\mathrm{m}$
Averaged PEB	$0.71\,\mathrm{m}$

VII. CONCLUSION

Regarding BLE-based indoor RSSI measurements, we showed the significant impact of the antenna patterns of off-the-shelf devices and that for moving agents in our setups, this distortion can be modelled as an additional log-normally distributed random variable. We furthermore analyzed the impact

---

[3]The visible pattern of the RSSI measurements is caused by an additional moving average filter over three values for visualization purposes.

[4]All results were based on a single calibration walk, which followed a straight line through the anchor area from $\mathbf{p}_{\mathrm{start}} = \begin{bmatrix} 0, & 1.2 \end{bmatrix}^{\mathrm{T}}\,\mathrm{m}$ to $\mathbf{p}_{\mathrm{end}} = \begin{bmatrix} 14, & 1.2 \end{bmatrix}^{\mathrm{T}}\,\mathrm{m}$. Note that the calibration walk was conducted without high precision requirements and simply assumed a walk of constant velocity between start point $\mathbf{p}_{\mathrm{start}}$ and end point $\mathbf{p}_{\mathrm{end}}$.
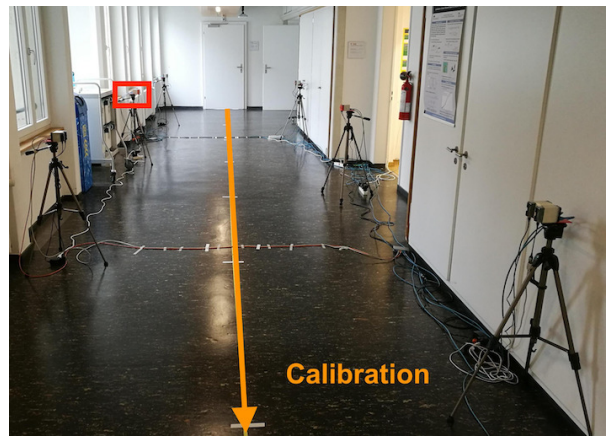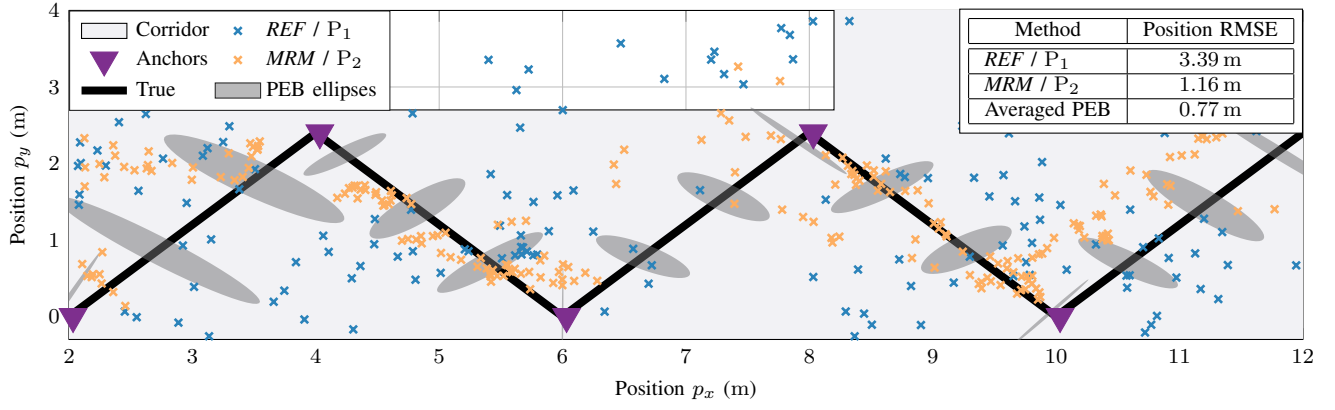
Fig. 9: Performance comparison for the position estimation for a zigzag trajectory through an office corridor.
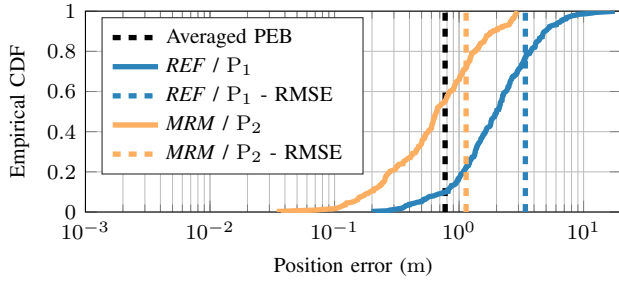

Fig. 10: Empirical CDF of the position estimation from Fig. 9.

of small-scale fading on RSSI-based distance estimation and showed that for Rayleigh fading at least 3 diversity branches should be used in order to sufficiently mitigate this impact. The analysis also confirmed that anchors close to the agent are more reliable and that high anchor densities are thus desirable. Moreover, we proposed a novel calibration scheme which allows to estimate different path loss exponents for distinct propagation environments and reduces the overall error variance of the distance estimates.

Combining the above information and schemes in a real world localization system for an office corridor reduced the position RMSE by 61% to 1.36 m. Furthermore, based on the measurements of our setup and the position error bound for the log-normal PLM, we determined a theoretically achievable RMSE of 0.71 m. Moreover, the presented schemes can also serve as a basis for temporal filtering or sensor fusion based systems in order to meet even higher accuracy demands.

VIII. ACKNOWLEDGMENTS

APPENDIX A
DISTANCE ERROR ESTIMATION

Due to the restriction to Rayleigh fading and the resulting scaled-χ^2-distribution of x with $2L$ degrees of freedom and non-centrality parameter $\lambda = 0$, we can easily calculate the expected value $\mathrm{E}\left[x^{-\frac{1}{\alpha}}\right]$ by integral substitution of $\frac{x}{2}$

$$\varepsilon_x(L, \alpha) := \mathrm{E}\left[x^{-\frac{1}{\alpha}}\right] \tag{22}$$

$$= \left(\frac{2L}{\sigma_h^2}\right)^{\frac{1}{\alpha}} \int_0^\infty \frac{x^{L-1}\exp(-\frac{x}{2})}{2^L\,\Gamma(L)}\, x^{-\frac{1}{\alpha}}\, \mathrm{d}x \tag{23}$$

$$= \left(\frac{L}{\sigma_h^2}\right)^{\frac{1}{\alpha}} \frac{\Gamma(L - \frac{1}{\alpha})}{\Gamma(L)}. \tag{24}$$

Note that the result (24) only holds for $L > \alpha^{-1}$.

REFERENCES

[1] A. Goldsmith, *Wireless Communications*. Cambridge University Press, 2005.

[2] Q. Dong and W. Dargie, "Evaluation of the Reliability of RSSI for Indoor Localization," in *Wireless Communications in Unusual and Confined Areas (ICWCUCA), 2012*. IEEE, 2012, pp. 1–6.

[3] M. Wadhwa, M. Song, V. Rali, and S. Shetty, "The impact of antenna orientation on wireless sensor network performance," in *Computer Science and Information Technology, 2009. ICCSIT 2009. 2nd IEEE International Conference on*, 2009, pp. 143–147.

[4] W. W.-L. Li, R. A. Iltis, and M. Z. Win, "A Smartphone Localization Algorithm using RSSI and Inertial Sensor Measurement Fusion," in *Global Communications Conference (GLOBECOM), 2013 IEEE*. IEEE, 2013, pp. 3335–3340.

[5] F. Zafari, I. Papapanagiotou, M. Devetsikiotis, and T. Hacker, "An iBeacon based Proximity and Indoor Localization System," *arXiv preprint arXiv:1703.07876*, 2017.

[6] Y. Qi, "Wireless Geolocation in a Non-Line-of-Sight Environment," Ph.D. dissertation, Princeton University, 2003.

[7] J. C. Liberti and T. S. Rappaport, "Statistics of Shadowing in Indoor Radio Channels at 900 and 1900 MHz," in *Military Communications Conference. MILCOM'92, Conf. Record. Communications-Fusing Command, Control and Intelligence., IEEE*. IEEE, 1992, pp. 1066–1070.

[8] Apple Inc., "iPhone 6 - Technical Specifications," accessed 2018-05-05. [Online]. Available: https://support.apple.com/kb/SP705

[9] RS Electronics, "Raspberry Pi 3 Model B," accessed 2018-05-05. [Online]. Available: http://docs-europe.electrocomponents.com/webdocs/14ba/0900766b814ba5fd.pdf

[10] Apple Inc., "iPod touch (5th generation)," accessed 2018-05-05. [Online]. Available: https://support.apple.com/kb/SP657

[11] S. D. Chitte, S. Dasgupta, and Z. Ding, "Distance Estimation From Received Signal Strength Under Log-Normal Shadowing: Bias and Variance," *IEEE Signal Processing Letters*, vol. 16, no. 3, 2009.

[12] Y. Shen, H. Wymeersch, and M. Z. Win, "Fundamental Limits of Wideband Localization Part II: Cooperative Networks," *IEEE Transactions on Information Theory*, vol. 56, no. 10, pp. 4981–5000, 2010.